S. Wu, N. Nishiyama, M. R. Kano, K. Itaka, U. -I. Chung, K. Kataoka,	Enhancement of Angiogenesis through Stabilization of Hypoxia Inducible Factor-1 by Silencing Prolyl Hydroxylase Domain 2 Gene. Mol Ther.	Mol Ther	16 (7)	1227-1234	2008
Y. Lee, K. Miyata, M. Oba, T. Ishii, S. Fukushima, M. Han, H. Koyama, N. Nishiyama, K. Kataoka,	Charge-conversion ternary polyplex with endosome disruption moiety: A technique for efficient and safe gene delivery. Angew. Chem.	Int. Ed.	47 (28)	5163-5166	2008
S. Takae, K. Miyata, M. Oba, T. Ishii, N. Nishiyama, K. Itaka, Y. Yamasaki, H. Koyama, K. Kataoka,	PEG-detachable polyplex micelles based on disulfide-linked block catiomers as bioresponsive nonviral gene vectors.	J. Am. Chem. Soc.	130 (18)	6001-6009	2008
K. Sugisaki, T. Usui, N. Nishiyama, W-D Jang, Y. Yanagi, S. Yamagami, S. Amano, K. Kataoka,	Photodynamic therapy for corneal neovascularization using polymeric micelles encapsulating dendrimer porphyrins.	Invest. Ophth. Vis. Sci.	49 (3)	894-899	2008
Suzuki R, Oda Y, Utoguchi N, Namai E, Taira Y, Okada N, Kadowaki N, Kodama T, Tachibana K, Maruyama K.	A novel strategy utilizing ultrasound for antigen delivery in dendritic cell-based cancer immunotherapy.,	J Cntrol Release.	133(3)	198-205	2009
Negishi Y, Endo Y, Fukuyama T, Suzuki R, Takizawa T, Omata D, Maruyama K, Aramaki Y.,	Delivery of siRNA into the cytoplasm by liposomal bubbles and ultrasound.	J Cntrol Release.	132(2)	124-130	2008
Suzuki R, Takizawa T, Negishi Y, Utoguchi N, Maruyama K.,	Effective gene delivery with novel liposomal bubbles and ultrasonic destruction technology.	Int J Pharm.	354(1-2)	49-55	2008
Zenitani T, Suzuki R, Maruyama K, Furuhata	H, Accelerating effects of ultrasonic thrombolysis with bubble liposomes,	J Med Ultrasonics,	35	5–10	2008
Tsuchihara K, et al.	Massive transcriptional start site analysis of human genes in hypoxia cells. Nucleic Acids Res.	Nucleic Acids Res.			Epub ahead of print. 2009

Tsuchihara K et al	Autophagy and cancer: Dynamism of the metabolism of tumor cells and tissues. Cancer Lett. Epub ahead of print. 2008	Cancer Lett			Epub ahead of print. 2008
Kuga W, Tsuchihara K et al.	Nuclear localization of SNARK; its impact on gene expression.	Biochem Biophys Res Commun	377	1062-6	2008
Tomasini R, Tsuchihara K et al.	TAp73 knockout shows genetic instability with infertility and tumor suppressor functions.	Genes Dev.	22	2677-91	2008
Tsuchihara K et al.	Susceptibility of Snark-deficient mice to azoxymethane-induced colorectal tumorigenesis and the formation of aberrant crypt foci.	Cancer Sci.	99	677-82	2008
Momose, I., Kunimoto, S., Osono, M., Ikeda, D.	Inhibitors of insulin-like growth factor-1 receptor tyrosine kinase are preferentially cytotoxic to nutrient-deprived pancreatic cancer cells.	Biochem. Biophys. Res. Commun	380	171-176	2009
Iljima, M., Momose, I., Ikeda, D.	TP-110, A new proteasome inhibitor, down-regulates IAPs in human multiple myeloma cells.	Anticancer Res	29		in press (2009)
Watanabe, T., Momose, I., Abe, M. Abe, H., Sawa, R., Umezawa, Y., Ikeda, D., Takahashi, Y., Akamatsu,Y,.	Synthesis of boronic acid derivatives of tyropeptin: proteasome inhibitors.	Bioorg. Med. Chem. Lett	19		in press (2009)
Kawada, M., Momose, I., Someno, T., Tsujiuchi, G., Ikeda, D	New atpenins, NBRI23477 A and B, inhibit growth of human prostate cancer cells.	J. Antibiotics	62		in press (2009)
Fujii S, Mitsunaga S, Yamazaki M, Hasebe T, Ishii G, Kojima M, Kinoshita T, Ueno T, Esumi H, Ochiai A.	Autophagy is activated in pancreatic cancer cells and correlates with poor patient outcome.	Cancer Sci	99(9)	1813-1819	2008

Ueno T, Sato W, HorieY, Komatsu M, Tanida I, Yoshida M , Ohshima S.	Mak TW, Watanabe S, Kominami E. Loss of Pten, a tumor suppressor, causes the strong inhibition of autophagy without affecting LC3 lipidation.	Autophagy	4(5)	692-700	2008

Int. J. Cancer: **124,** 2505–2511 (2009)

FAST TRACK

Potent antitumor effect of SN-38-incorporating polymeric micelle, NK012, against malignant glioma

Jun-ichiro Kuroda[1,2], Jun-ichi Kuratsu[2], Masahiro Yasunaga[1], Yoshikatsu Koga[1], Yohei Saito[1] and Yasuhiro Matsumura[1]*

[1]*Investigative Treatment Division, Research Center for Innovative Oncology, National Cancer Center Hospital East, Kashiwa, Japan*
[2]*Department of Neurosurgery, Faculty of Medical and Pharmaceutical Sciences, Kumamoto University, Kumamoto, Japan*

Recent published reports on clinical trials of CPT-11 indicate the effectiveness of this compound, a prodrug of SN-38, against malignant glioma in combination with anti-vascular endothelial growth factor antibody. Here, we determined if NK012, and SN-38 incorporating micelle, can be an appropriate formulation for glioblastoma treatment compared with CPT-11. *In vitro* cytotoxicity was evaluated against several glioma lines with NK012, CPT-11, SN-38, ACNU, CDDP and etoposide. For the *in vivo* test, a human glioma line (U87MG) transfected with the *luciferase* gene was inoculated into nude mice brain for pharmacokinetic analysis by fluorescence microscopy and high-performance liquid chromatography after intravenous injection of NK012 and CPT-11. *In vivo* antitumor activity of NK012 and CPT-11 was evaluated by bioluminescence image and Kaplan-Meier analyses. The growth-inhibitory effects of NK012 were 34- to 444-fold more potent than those of CPT-11. Markedly enhanced and prolonged distribution of free SN-38 in the xenografts was observed after NK012 injection compared with CPT-11. NK012 showed significantly potent antitumor activity against an orthotopic glioblastoma multiforme xenograft and significantly longer survival rate than CPT-11 ($p = 0.0014$). This implies that NK012 can pass through the blood brain tumor barrier effectively. NK012, which combines enhanced distribution with prolonged sustained release, may be ideal for glioma treatment. Currently, a phase I study of NK012 is almost complete in Japan and the US. The present translational study warrants the clinical phase II study of NK012 in patients with malignant glioma.

Key words: glioma; drug delivery system; blood brain barrier (BBB); SN-38; micelles

Malignant astrocytomas, such as anaplastic astrocytoma and glioblastoma multiforme (GBM), are the most common and highly vascularized glial tumors of the brain. At least 80 percent of malignant gliomas are categorized as GBM.[1] Currently, GBM patients have a mean survival of only 50 weeks following the standard treatment consisting of surgical and adjuvant therapies.[2] A recent phase III randomized trial for newly diagnosed GBM demonstrated that radiation therapy with concurrent temozolomide treatment, followed by 6 months of temozolomide treatment was superior to radiation therapy alone in terms of overall survival.[3] In addition, several clinical trials have demonstrated that the median survival times of patients with recurrence were only 3–6 months.[4]

The anticancer plant alkaloid 7-ethyl-10-hydroxy-camptothecine (SN-38) is a broad spectrum anticancer agent targeting DNA topoisomerase I with a different mechanism of action compared with alkylating agents such as temozolomide. Although SN-38 has shown promising anticancer activity *in vitro* and *in vivo*, its clinical application has remained dormant because of its low therapeutic efficacy and severe toxic effects.[5,6] Irinotecan hydrochloride (CPT-11), a prodrug of SN-38, shows some antitumor activities in patient with recurrent GBM, with response rates of 0 to 17% in several trials.[7–10] CPT-11 activity is thus similar to that of other agents used for recurrent GBM.[9] A recent phase II trial for recurrent GBM demonstrated that the combination of CPT-11 and bevacizumab, an antivascular endothelial growth factor (VEGF) monoclonal antibody, is an effective treatment against the neoplasia with a 6-month progression-free survival rate of 46% and a 6-month overall survival rate of 77%.[11,12] However, there is an increased risk of developing venous thromboembolic disease and intracranial hemorrhage with this combination therapy. Therefore, there is an urgent need to develop treatment modalities by which cytotoxic drugs can exert more potent antitumor activity to their full potential with modest adverse effects and thereby reasonably prolong the overall survival in GBM patients.

The purpose of the drug delivery system (DDS) is to achieve selective delivery of antitumor agents to tumor tissue at an effective concentration for the appropriate duration of time in order to reduce the adverse effects of the administered drug and simultaneously enhance its antitumor effect. There are 2 main concepts in DDS, active targeting and passive targeting. Active targeting involves a monoclonal antibody and a ligand to a tumor-related receptor. Doxil, a doxorubicine incorporated polyethylene glycol conjugated liposome, is categorized under passive targeting agents and are already in clinical use.[13,14] NK012, a novel SN-38-incorporating polymeric micelle, is a prodrug of SN-38 similar to CPT-11 and categorized under passive targeting agent as well. Although CPT-11 is converted to SN-38 in tumors by carboxylesterase (CE), the metabolic conversion rate is within 2–8% of the original volume of CPT-11.[15,16] In contrast, the release rate of SN-38 from NK012 is 74% under physiologic pH condition even without CEs.[17] Recently, we have demonstrated that NK012 exerted significantly more potent antitumor activity against various human tumor xenografts than CPT-11.[17–20] However, there is a fundamental question whether such nanoparticles can reach brain tumors across the tumor microvessels. In the present study, therefore, we established an orthotopic glioma model in this experiment and then evaluated whether NK012 can pass through the BTB and exert its antitumor effect on orthotopic human glioma xenografts in comparison with CPT-11.

Material and methods

Drugs

NK012 and SN-38 were donated by Nippon Kayaku Co., Ltd. (Tokyo, Japan). The size of NK012 was ~20 nm in diameter with a narrow size distribution.[17] ACNU [1-(4-amino-2-methyl-5-pyrimidinyl) methyl-3-(2-chloroethyl)-3-nitrosourea, nimstine] was purchased from DAIICHI SANKYO Co., Ltd. (Tokyo, Japan). CDDP (cis-diamminedichloroplatinum) and CPT-11 were purchased from Yakult Co., Ltd. (Tokyo, Japan). Etoposide [4′demethlepipodophyllotoxin-9-(4, 6-O-ethylidene-β-D-glucopyranoside)] was purchased from BIOMOL (Plymouth Meeting, PA).

Grant sponsors: Ministry of Health, Labour and Welfare of Japan (Third Term Comprehensive Contorol Research for Cancer), Core Research for Evolutional Science and Technology, Ministry of Education, Culture, Sports, Science and Technology.

***Correspondence to:** Investigative Treatment Division, Research Center for Innovative Oncology, National Cancer Center Hospital East, 6-5-1 Kashiwanoha, Kashiwa 277-8577, Japan. Fax: +81-4-7134-6857. E-mail: yhmatsum@east.ncc.go.jp.

Received 10 September 2008; Accepted after revision 28 October 2008
DOI 10.1002/ijc.24171
Published online 24 November 2008 in Wiley InterScience (www.interscience.wiley.com).

Cells and animals

Five human glioma cell lines, namely U87MG, U251MG, U118MG, LN18 and LN229, were obtained from the American Type Culture Collection (Rockville, MD). Cells were maintained in Dulbecco's modified Eagle's minimum essential medium supplemented with 10% fetal bovine serum (Cell Culture Technologies, Gaggenau-Hoerden, Germany), penicillin, streptomycin and amphotericin B (100 units/ml, 100 μg/ml and 25 μg/ml, respectively; Sigma, St. Louis, MO) in a humidified atmosphere containing 5% CO_2 at 37°C. Six- to eight-week-old athymic nude mice (nu/nu; Charles River Japan, Kanagawa, Japan) were used for this study. U87MG cells (1×10^5) were injected into the cerebral hemisphere using a Hamilton syringe through an entry point 1 mm anterior and 1.8 mm lateral to the bregma to an intraparenchymal depth of 2.5 mm. The rate of injection was 0.5 μl/min, and the needle was left in place for 5 min after completion of the injection. All animal procedures were performed in compliance with the Guidelines for the Care and Use of Experimental Animals established by the Committee for Animal Experimentation of the National Cancer Center, Japan; these guidelines meet the ethical standards required by law and also comply with the guidelines for the use of experimental animals in Japan.

Establishment of U87MG cell line stably expressing firefly luciferase and YFP mutant Venus

For the *in vivo* bioluminescence imaging of orthotopic brain tumors, the U87MG cell line stably expressing firefly luciferase and the YFP mutant Venus was established. Briefly, the coding sequence for firefly luciferase and Venus was subcloned into the the pIRES Vector (Clontech Laboratories, Mountain View, CA). The fragment consists of Luciferase-IRES-Venus generated from the plasmid with the restriction enzymes Nhe I and Not I. This fragment was subcloned into the pEF6/V5-His Vector (Invitrogen, Carlsbad, CA) to generate plasmids of pEF6-Lucifease IRES Venus. U87MG cells (2×10^6) were seeded onto 10-cm dishes 24 hr before transfection. The cells were transfected with 10 μg of pEF6-Lucifease IRES Venus using FuGENE HD Transfection Reagent (Roche Diagnostics, Mannheim, Germany) according to manufacturer's instructions, and then incubated for 48 hr at 37°C. The cells were then passaged in medium containing Blasticidin (10 μg/ml; InvivoGen, San Diego, CA) to select for the Blasticidin resistance gene integrated in the pEF6/V5-His plasmids. Venus expression was used as a surrogate marker of luciferase-positive cells. Venus-expressing U87MG cells (U87MG/Luc) were sorted using the BD FACS Aria cell sorter (BD Biosciences, San Jose, CA), and expanded in selection medium. The accuracy of a quantitive bioluminescence image as an indicator of U87MG/Luc cell number was analyzed using the Photon Imager animal imaging system *in vitro*, as described under *in vivo* growth inhibition assay. This analysis demonstrated clear correlation between a quantitive bioluminescence image and cell number ($R^2 = 0.99$). The sensitivity of U87MG/Luc cells to each drug (NK012, CPT-11, SN-38, ACNU, CDDP and etoposide) was almost similar to that of parental U87MG cells (data not shown).

In vitro *growth inhibition assay*

Cell growth inhibition was measured by the tetrazolium salt-based proliferation assay (WST assay; Wako Chemicals, Osaka, Japan). Briefly, cells (5×10^3 cells/well) in 96-well plates were incubated overnight. Then, growth medium was changed to new medium with various concentrations of SN-38, NK012, CPT-11, ACNU, etoposide and CDDP. After 72 hr of incubation, medium was changed to new medium containing 10% WST-8 reagents. After 1 hr of incubation, the absorbance of the formazan product formed was detected at 450 nm in a 96-well spectrophotometric plate reader (SpectraMax 190; Molecular Devices, Sunnyvale, CA). Cell viability was measured and compared with that of the control cells. Each experiment was carried out in triplicates and was repeated at least 3 times. Data were averaged and normalized against the nontreated controls to generate dose-response curves. The number of living cells (% Control) was calculated using the following formula: % Control = (each absorbance—absorbance of blank well)/absorbance of control well × 100.

Evaluation of NK012 and CPT-11 distribution in tumor tissue by fluorescence microscopy

The U87MG orthotopic xenograft model described earlier was used for the analysis of the biodistribution of NK012 and CPT-11. Twenty days after U87MG/Luc inoculation, the maximum tolerated dose (MTD) of NK012 (30 mg/kg) or CPT-11 (66.7 mg/kg) was injected intravenously into the tail vein of mice. At this point, tumor size reached to about 3 mm in diameter according to the preliminary experiment (data not shown). Two, 12 or 24 hr after NK012 or CPT-11 injection, mice were also administered with fluorescein *Lycopersicon esculentum* lectin (100 μl/mouse) (Vector Laboratories, Burlingame, CA) to visualize tumor blood vessels. Tumors were then excised and embedded in optimal cutting temperature compound and frozen at −80°C until use. Tissue sections (6 μm thick) were prepared using Tissue-Tek Cryo3 (Sakura Finetek USA, Inc., Torrance, CA), and frozen sections were examined under a fluorescence microscope, BIOREVO BZ9000 (Keyence, Osaka, Japan), at an excitation wavelength of 377 nm and an emission wavelength 447 nm to evaluate the distribution of CPT-11 and NK012 within the tumor tissues. Because formulations containing SN-38 bound *via* ester bonds possess a particular fluorescence, both CPT-11 and NK012 were detected under the same fluorescence conditions. Image data were recorded using BZ-II Analyzer 1.10 software (Keyence, Osaka, Japan).

Pharmacokinetics study of NK012 and CPT-11

Female BALB/c nude mice bearing U87MG/Luc tumor ($n = 3$) were used for the analysis of the biodistribution of NK012 and CPT-11. Twenty days after the intracranial injection of U87MG/Luc cells, NK012 (30 mg/kg) or CPT-11 (66.7 mg/kg) was intravenously administered to the mice. Under anesthesia, blood, normal brain tissues and tumor tissues were obtained 2, 12, 24 and 72 hr after NK012 or CPT-11 administration. Blood samples were collected in microtubes and immediately centrifuged at 1,600*g* for 15 min at 4°C. All samples were stored at −80°C until use.

The normal brain and tumor samples were rinsed with physiologic 0.9% NaCl solution, mixed with 0.1 M glycine-HCl buffer (pH 3.0)/methanol at 5 w/w%, and then homogenized. To analyze the concentration of free SN-38 and CPT-11, 100 μl of the tumor homogenates was mixed with 20 μl of 1 mM phosphoric acid/methanol (1:1), 40 μl of ultrapure water and 60 μl of camptothecin solution (10 ng/ml for SN-38 and 15 ng/ml for CPT-11) as an internal standard. To quantify free SN-38 and CPT-11 in plasma, 25 μl of plasma was mixed with 25 μl of 0.1 M HCl, and then added with 20 μl of 1 mM phosphoric acid/methanol (1:1) and 100 μl of CPT solution (10 ng/ml both for SN-38 and CPT-11). The samples were vortexed vigorously for 10 sec, and then filtered through Ultrafree-MC centrifugal filter devices with a cut-off molecular diameter of 0.45 μm (Millipore Co., Bedford, MA). Reversed-phase HPLC was performed at 35°C on a Mightysil RP-18 GP column 150 × 4.6 mm^2 (Kanto Chemical Co., Inc., Tokyo, Japan). Fifty microliters of a sample was injected into an Alliance Waters 2795 HPLC system (Waters, Milford, MA) equipped with a Waters 2475 multi λ fluorescence detector. Fluorescence originating from SN-38 was detected at 540 nm with an excitation wavelength of 365 nm and that originating from CPT-11 was detected at 430 nm with an excitation wavelength of 365 nm. The mobile phase was a mixture of 100 nmol/l ammonium acetate (pH 4.2) and methanol (11:9 (v/v)). The flow rate was 1.0 ml/min. The content of SN-38 was calculated by measuring the relevant peak area and calibrating against the corresponding peak area derived from the CPT internal standard. Peak data were recorded using a chromatography management system (MassLynx v4.0, Waters).

For polymer-bound SN-38 detection, SN-38 was released from the conjugate. Briefly, 20 μl of plasma and 100 μl of tissue

TABLE I – IC_{50} VALUES OF SN-38, NK012, CPT-11, ACNU, CDDP AND VP-16 IN VARIOUS HUMAN GLIOBLASTOMA CELL LINES

Cell line	IC_{50}(μmol/l)					
	SN38	NK012	CPT-11	ACNU	CDDP	Etoposide
LN18	0.052 ± 0.0034	0.069 ± 0.0242	13.0 ± 0.88	729 ± 30	3.57 ± 0.08	3.84 ± 0.14
LN229	0.28 ± 0.1094	0.36 ± 0.0489	12.2 ± 1.23	144 ± 23	21.4 ± 0.62	0.945 ± 0.025
U87MG	0.18 ± 0.0216	0.093 ± 0.0038	18.1 ± 3.06	865 ± 86	9.06 ± 0.57	20.8 ± 5.23
U118MG	0.0089 ± 0.0003	0.022 ± 0.0017	4.85 ± 0.14	282 ± 22	3.35 ± 0.35	4.05 ± 0.18
U251MG	0.0076 ± 0.0001	0.0087 ± 0.0002	3.86 ± 0.04	51.6 ± 3.7	4.55 ± 0.03	2.42 ± 0.13

Each cell line was treated in triplicate for 72 hr.
WST–8 assay was used for obtaining IC_{50} value.

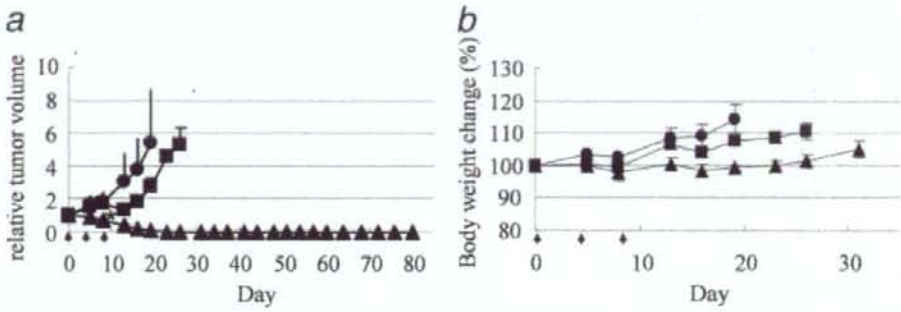

FIGURE 1 – Effects of NK012 and CPT-11 on U87MG/Luc tumor xenograft. (*a*) Tumor volume in mice treated with CPT-11 or NK012. U87MG/Luc tumor was subcutaneously inoculated into the flank of mice, as described in the Materials and methods section. NaCl (0.9%) solution (●), CPT-11 at 66.7 mg/kg (■) and NK012 at 30 mg/kg (▲) were intravenously administered on days 0, 4 and 8 (arrows). Points, mean; bars, SD. $*p < 0.05$. (*b*) Treatment-related body weight loss occurred in mice treated with CPT-11 and NK012. Points, mean; bars, SD.

samples were diluted with 20 μl of methanol (50%, v/v) and 20 μl of NaOH (0.3 mol/l for plasma and 0.7 mol/l for tissue). The samples were incubated for 15 min at 25°C. After incubation, 20 μl of HCl (0.3 mol/l for plasma and 0.7 mol/l for tissue) and 60 μl of CPT solution (10 ng/ml for SN-38 and 15 ng/ml for CPT-11) were added to the samples, and then the hydrolysate was filtered through a MultiScreen Solvinert. Fifty microliters of the filtrate was applied to the same HPLC system as described earlier.

In vivo *growth inhibition assay*

Experiment 1. Six-week-old mice were subcutaneously inoculated with 1×10^7 U87MG/Luc cells in the flank region. When tumor volume reached ~605 mm^3, mice were randomly divided into test groups consisting of 3 mice per group (day 0). Drug was intravenously administered on days 0, 4 and 8 into the tail vein. NK012 was administered at its MTD of 30 mg/kg/day. The reference drug CPT-11 was given at its MTD of 66.7 mg/kg/day in the optimal schedule reported.[17,21] The length (*i*) and width (*ii*) of tumor masses were measured twice a week, and tumor volume (TV) was calculated as follows: $TV = (a \times b^2)/2$. Relative tumor volumes (RTVs) at day *n* were calculated according to the following formula: $RTV = TV_n / TV_0$, where TV_n is the tumor volume at day *n*, and TV_0 is the tumor volume at day 0.

Experiment 2. To assess the antitumor effect of NK012 and CPT-11, *in vivo* bioluminescence imaging studies were performed using the Photon Imager animal imaging system (Biospace, Paris, France). For imaging, mice with intracranial U87MG/Luc tumor were simultaneously anesthetized with isoflurane and *d*-luciferine potassium salt (Synchem, Germany), and normal 0.9% NaCl solution was intraperitoneally administrated at a dose of 125 mg/kg body weight, and images were obtained 5 min after the injection. For bioluminescence image analysis, regions of interest encompassing the intracranial area of a signal were defined using Photo Vision software (Biospace, Paris, France), and total numbers of photons per minute (cpm) were recorded. The pseudo-color luminescent image from violet (least intense) to red (most intense) represented the spatial distribution of detected photon counts emerging from active luciferase within the animal. Twenty days after U87MG inoculation, treatment was started (day 0). Normal 0.9% NaCl solution ($n = 4$), NK012 (30 mg/kg, $n = 4$), or CPT-11 (66.7 mg/kg, $n = 4$) was intravenously administered to mice on days 0, 4 and 8. *In vivo* bioluminescence imaging studies were performed on days 0, 14, 21 and 28 from the day of treatment initiation. To determine the effect of treatment on the time to change of intensity, Student's *t* test was carried out using the StatView 5.0 software package. $p < 0.05$ was regarded as significant.

Experiment 3. Mice with intracranial U87MG/Luc tumor was randomly divided into 3 groups consisting of 6 mice per group. NK012 (30 mg/kg/day) and CPT-11 (66.7 mg/kg/day) were intravenously given on days 0 (20 days after tumor inoculation), 4 and 8. After treatment, mice were maintained until each animal showed signs of morbidity (*i.e.*, 10% weight loss and neurological deficit), at which point they were sacrificed. Kaplan-Meier analysis was performed to determine the effect of drugs on time to morbidity, and statistical differences were ranked according to the Mantel-Cox log-rank test using StatView 5.0.

Statistical analysis

Data were expressed as mean ± SD. Significance of differences was calculated using the unpaired *t* test with repeated measures of StatView 5.0. $p < 0.05$ was regarded as significant.

Results

Cellular sensitivity of glioblastoma cells to SN-38, NK012 and CPT-11

The IC_{50} values of NK012 for the cell lines ranged from 0.0087 μmol/l (U251MG cells) to 0.36 μmol/l (LN229 cells). The growth inhibitory effects of NK012 were 34- to 444-fold more potent than those of CPT-11, 400- to 12818-fold more potent than those of ACNU, 52-to 523-fold more potent than those of CDDP, and 3- to 278-fold

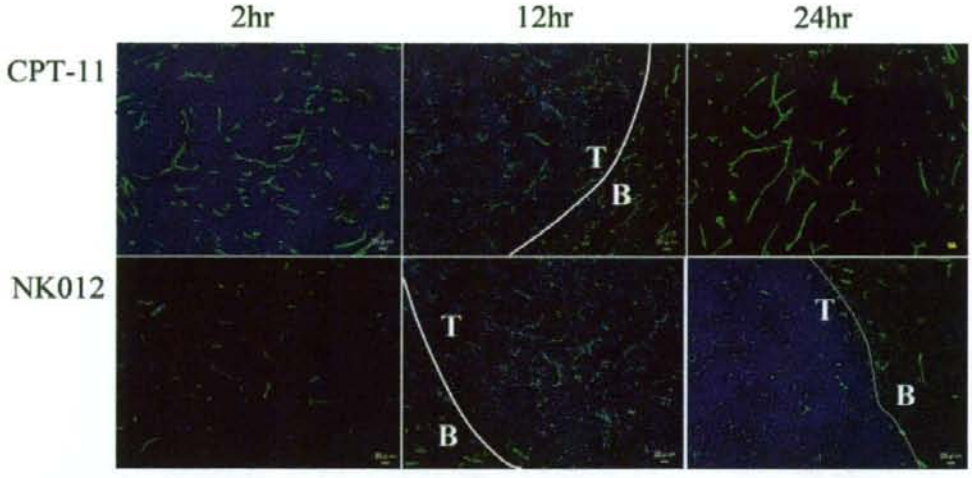

FIGURE 2 – Distribution of NK012 or CPT-11 in U87MG/Luc glioma xenografts. Mice bearing U87MG/Luc tumor were injected with NK012 (30 mg/kg/day) or CPT-11 (66.7 mg/kg/day). Tumor tissues were excised 2, 12 and 24 hr after the intravenous injection of NK012 or CPT-11. Each mouse was administered fluorescein-labeled *Lycopersicon esculentum* lectin 5 min before sacrifice to detect tumor blood vessels. Frozen sections were examined under a fluorescence microscope at an excitation wavelength of 377 nm and an emission wavelength of 477 nm. The same fluorescence conditions can be applied for visualizing NK012 and CPT-11 fluorescence. Free SN-38 could not be detected under these fluorescence conditions. The white lines indicate the border between the tumor and the brain tissue. T, U87MG/Luc tumor; B, normal brain tissue. (Scale bars: 20 μm).

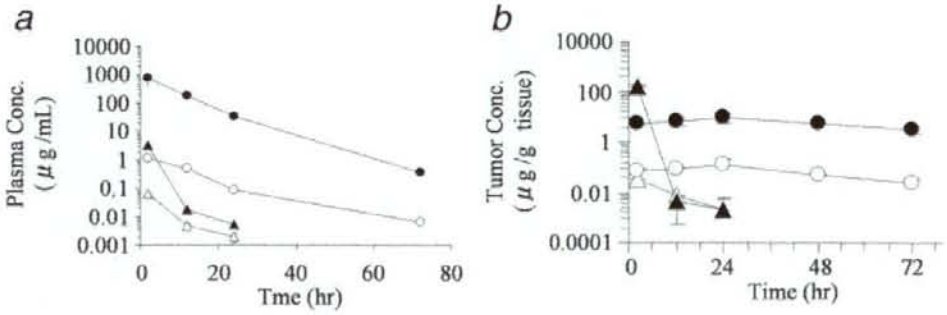

FIGURE 3 – Plasma, brain tissue and orthotopic tumor concentrations of respective analytes after intravenous administration of NK012 (30 mg/kg/day) and CPT-11 (66.7 mg/kg/day) to U87MG/Luc-bearing nude mice. (*a*) plasma; (*b*) tumor. ●, polymer-bound SN-38; ○, free SN-38 (polymer-unbound SN-38); ▲, CPT-11; Δ, free SN-38 converted from CPT-11.

more potent than those of etoposide. On the other hand, the IC_{50} values of NK012 were almost similar to those of SN-38 (Table. I).

Antitumor activity of NK012 and CPT-11 on subcutaneous U87MG/Luc xenografts

Potent antitumor activity was observed in mice treated with NK012 at 30 mg/kg *in vivo* (Fig. 1*a*). In mice treated with NK012, tumor volume started to decrease on day 5, and the tumor completely disappeared by day 23, with no relapse observed until 80 days after treatment. Although CPT-11 at 66.7 mg/kg/day exerted antitumor activity compared with the control group, tumor volume continued to increase consistently. Comparison of the relative tumor volume at day 8 revealed significant differences between the NK012-treated and CPT-11-treated groups ($p = 0.0095$). Although treatment-related body weight loss was observed in mice treated with each drug, body weight recovery was observed by day 19 (Fig. 1*b*). These results clearly show the significant *in vivo* activity of NK012 against the U87MG/Luc tumor xeonograft.

Studies on distribution of NK012 and CPT-11 in orthotopic U87MG/Luc tumor tissues

Both NK012 and CPT-11 formulations accumulated in the tumor tissue but not in the normal brain tissue (Fig. 2). However, the drug distribution pattern was clearly different between NK012 and CPT-11. In sections of the U87MG/Luc tumor treated with CPT-11, maximum drug accumulation was observed within 2 hr of CPT-11 injection. Twelve hours after the injection, fluorescence originating from CPT-11 had almost disappeared. Subsequently, no accumulation of CPT-11 was observed within the tumor tissues. However, in sections of the U87MG/Luc tumor treated with NK012, fluorescence from NK012 started appearing around tumor blood vessels 2 hr after intravenous injection and lasted until 24

TABLE II – TUMOR AND PLASMA CONCENTRATION OF SN38 AFTER AN I.V. ADMINISTRATION OF NK012 (30 MG/KG) AND CPT-11 (66.7MG/KG) TO NUDE MICE BEARING U87MG/LUC BRAIN TUMOR

Formulation tested	Analyte		Time after administration (hr)			
			2	12	24	72
NK012	Free SN-38	Plasma (ng/ml)	1113	511	90.0	6.88
		Tumor (ng/g)	67.7	84.1	137	24.6
CPT-11	Free SN-38 5	Plasma (ng/ml)	62.0	4.74	1.97	ND
		Tumor (ng/g)	31.8	7.41	2.14	ND

Data were expressed as means of three mice.
Free SN-38; SN-38 released from NK012 or converted from CPT-11.
ND, not detectable.

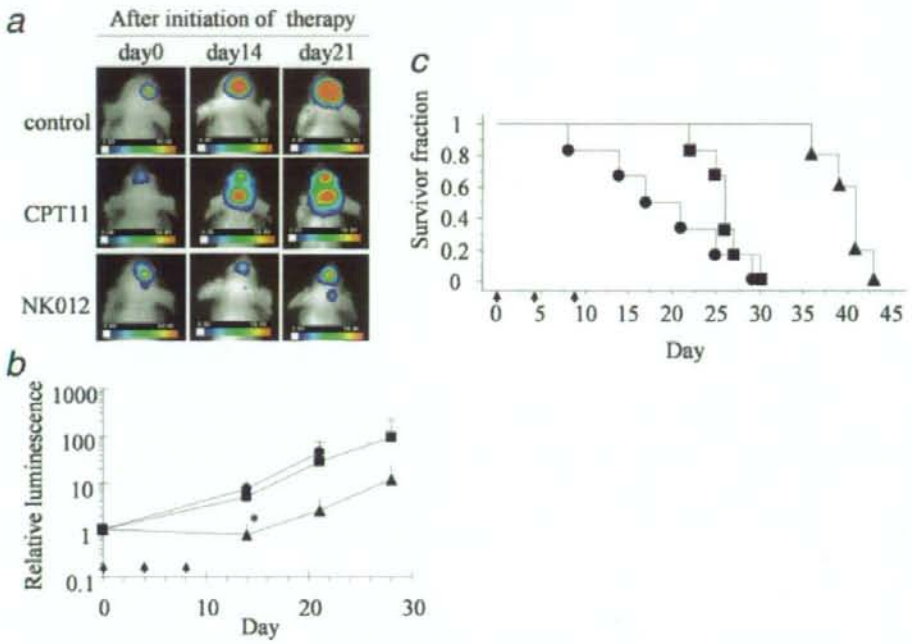

FIGURE 4 – Antitumor effect of NK012 or CPT-11 on orthotopic xenograft and survival. Mice receiving intracranial injections of U87MG/Luc were assigned into groups 20 days after tumor inoculation. Mice were intravenously administered with 0.9% NaCl solution (●), NK012 (30 mg/kg/day, ▲) or CPT-11 (66.7 mg/kg/day, ■) on days 0 (20 days after tumor inoculation), 4 and 8 (arrows). (*a*) Representative luminescence intensity images obtained in individual control and treatment-group mice on the days indicated. (*b*) Antitumor effect of NK012 or CPT-11 on days 14, 21 and 28. Each group consisted of 4 mice. Points, mean; bars, SD. $*p < 0.05$. (*c*) Treatment effects of NK012 on survival. Survival was assessed by Kaplan-Meier analysis. Each group consisted of 6 mice. Experiments were repeated twice with similar results.

hr. After 12 hr, the fluorescent area began to increase and the maximum fluorescence area was observed 24 hr after the injection.

Pharmacokinetics analysis of NK012 and CPT-11 in mice bearing orthotopic U87MG/Luc xenografts

Microscopic observations were confirmed quantitatively by measuring the amount of SN-38 extracted from each solid tumor by reversed-phase HPLC. After CPT-11 injection, the concentrations of CPT-11 and free SN-38 in plasma decreased rapidly with time in a log-linear fashion. On the other hand, the plasma concentration of NK012 (polymer-bound SN-38) showed slower clearance than that of CPT-11. Free SN-38 released from NK012 also showed slow clearance than that of SN-38 converted from CPT-11 (Fig. 3*a*). Meanwhile, there was a significant difference in drug accumulation in the tumor between CPT-11 and NK012, that is, the accumulation of NK012 in the U87MG/Luc tumor was significantly higher than that of CPT-11 (Fig. 3*b*) and that the concentration of free SN-38 originating from NK012 was maintained at 24.6 ng/g even 72 hr after injection (Table II). On the other hand, only slight conversion from CPT-11 to SN-38 was observed from 2 to 24 hr in the U87MG/Luc tumor, and no SN-38 was detected thereafter (Fig. 3*b*). This result suggests that the BTB of the tumor was partially destroyed in the tumor vasculature and both drugs extravasated from the tumor blood vessels. In addition, these results indicate that NK012 can remain in the tumor tissue for a longer period and continue to release free SN-38.

Antitumor activity of NK012 and CPT-11 against orthotopic U87MG/Luc glioma xenografts

Antitumor activity was observed in mice treated with NK012 at 30 mg/kg/day and CPT-11 at 66.7 mg/kg/day *in vivo* (Fig. 4*a*). ANOVA analysis revealed a significant difference between the control group and the NK012-treated group ($p = 0.02$). However there was no significant difference between the control group and

the CPT-11-treated group ($p = 0.23$) and between NK012 and CPT-11 ($p = 0.21$) (Fig. 4*b*). Comparison of the relative tumor volume at day 14 revealed significant differences between NK012 (30 mg/kg/day) and CPT-11 (66.7 mg/kg/day) ($p = 0.049$). Kaplan-Meier analysis showed that a significant improvement in survival rate was observed in the NK012 treatment group compared with the control ($p = 0.001$) and CPT-11 treatment groups ($p = 0.0014$) (Fig. 4*c*).

Discussion

The diameter of a micelle carrier is approximately in the range of 10–100 nm, which is smaller than that of a liposome. Although this size is small, it is still sufficiently large to prevent renal secretion of the carrier. The micelle systems can evade nonspecific capture by the reticuloendothelial system in various organs because the outer shell of the micelle is covered with polyethyleneglycol. Therefore, drug-incorporating micelles can be expected to have a long plasma half-life, which permits a large amount of the micelles to reach tumor tissues, extravasate from tumor capillaries, and then be retained in tumor tissues for a long time by utilizing the enhanced permeability and retention (EPR) effect.[22]

Several factors are reportedly involved in vascular permeability in the body. Among them, bradykinin is the most potent vascular permeability factor. We succeeded in purifying 2 types of kinin from the ascitic fluid of a patient with gastric cancer.[23] We also clarified that this kinin generation system was triggered by the activated Hageman factor, an intrinsic coagulation factor XII.[24] Meanwhile, Dvorak et al. discovered that the vascular permeability factor (VPF) is involved in tumor vascular permeability.[25] Later, it was found that VPF was identical to VEGF.[26] Recently, an extrinsic coagulation factor, namely, a tissue factor, has been shown to activate VEGF production.[27,28] Thus, both intrinsic and extrinsic coagulation factors may be involved in tumor vascular permeability. Furthermore, there have been several reports to date indicating the increasing expression of a tissue factor in human glioma.[29,30] Also, it is well known that glioma is a typical hypervascular tumor with an irregular vascular architecture and a high expression level of VEGF.[31] Therefore, it may be speculated that nanoparticles extravasate from tumor capillaries and accumulate more preferentially in brain glioma.

NK012, an SN-38-incorporating polymeric micelle, is a novel type of micellar formulation with long-time accumulation in tumors, and shows prolonged sustained release of SN-38 within the tumor.[17,20] We have thus far reported that NK012 shows significantly higher antitumor activity against various human tumor xenografts including small cell lung cancer,[17] colorectal cancer,[19] renal cancer,[18] and pancreatic cancer[20] compared with CPT-11. In addition, we have recently seen an increasing number of reports of clinical trials indicating the effectiveness of CPT-11 against brain glioma in combination with anti-VEGF antibody[11,12,32,33]

Under these circumstances, it may be reasonable to conduct an investigation into the advantages of administering NK012 over CPT-11 for treatment against human glioma tumor xenografts. In the present study, we showed that NK012 exerted a significant antitumor activity in U87MG/Luc subcutaneous xenografts (Fig. 1). In the tumor intravenously administered with NK012 (30 mg/kg), NK012 accumulated within and around tumor blood vessels in the orthotopic xenografts 2 hr after the injection. Thereafter, NK012 started to spread from the blood vessel within the tumor tissue of the xenografts. Fluorescence originating from NK012 then increased up to the maximum in the entire tumor by 24 hr after NK012 injection. On the other hand, fluorescence originating from CPT-11 increased up to the maximum 2 hr after its injection, indicating that the maximum distribution of CPT-11 was achieved within 2 hr of injection. Twelve hours after intravenous injection, fluorescence from CPT-11 had almost disappeared, and subsequently, no accumulation of CPT-11 was observed within the tumor tissues. The therapeutic effect of NK012 was superior to that of CPT-11 in terms of antitumor effect and survival. Because the antitumor activity of SN-38 is time-dependent, the superiority of NK012 over CPT-11 may be due to the enhanced accumulation of NK012 and the prolonged sustained release of SN-38 from NK012 within the tumor tissues. Nevertheless, free SN-38 was not detected in the normal brain tissues at any measurement time after intravenous injection of NK012 or CPT-11 (data not shown). It is thus speculated that both NK012 and CPT-11 are unable to cross the BBB in the normal brain, but can pass through tumor vessels effectively. In clinical brain glioma, however, when the tumor recurs, it would most likely recur in adjacent regions of the brain with an intact blood brain barrier. Namely, at the border between the brain tumor and normal brain tissue, malignant glioma cells and normal brain tissues intermix in the gradient and angiogenesis occurs at sites where there are large accumulation of tumor cells under local hypoxia.[34] In addition, there is no clear evidence if tumor vessels of orthotopic brain tumor xenografts are identical to those of real human brain tumors in terms of their structure and function. Therefore, it may be better to consider to conduct an investigation of the advantages of administering some anti-angiogenic inhibitors in combination with NK012 against highly invasive tumor models established by several methods such as direct implantation of patient surgical specimens into the brains of nude mice,[35] transplantation of patient surgical material s.c. in nude mice followed by dissociation and orthotopic reinjection of these xenotransplants,[36] engraftment of glioblastoma-derived spheroids after short- term culture into rat brain,[37] and engraftment of glioblastomastem cell-enriched cultures into mouse brain.[38,39]

The dose-limiting toxicities of CPT-11 appeared to be neutropenia and diarrhea. However, in our previous data, there was no significant difference in the level of SN-38 in the small intestine between NK012-treated and CPT-11-treated mice.[17] It was also reported that NK012 showed significant antitumor effect with diminishing incidence of diarrhea compared with CPT-11.[40] In 2 individual phase 1 trials in Japan and the US, no serious diarrhea has been reported.[41,42] In addition, one confirmed partial response (PR) was obtained in a patient with metastatic esophageal cancer in a Japanese trial,[41] and 3 PRs in a patient with breast cancer and 1 PR in a patient with small cell lung cancer in a US phase 1 trial.[42]

In conclusion, we demonstrated not only the enhanced accumulation, distribution, and retention of NK012 within glioma xenografts but also the superiority of the antitumor activity of NK012 compared with CPT-11. Taking the present data together with very recent clinical data from phase 1 trials, a phase 2 trial in patients with recurrent glioma may be warranted.

Acknowledgements

The authors thank Ms. N. Mie, Ms. H. Miyatake and Ms. M. Ohtsu for their technical assistance and Ms. K. Shiina for her secretarial assistance.

References

1. DeAngelis LM. Brain tumors. N Engl J Med 2001;344:114–23.
2. Kleihues P, Louis DN, Scheithauer BW, Rorke LB, Reifenberger G, Burger PC, Cavenee WK. The WHO classification of tumors of the nervous system. J Neuropathol Exp Neurol 2002;61:215–25 discussion 26–9.
3. Stupp R, Mason WP, van den Bent MJ, Weller M, Fisher B, Taphoorn MJ, Belanger K, Brandes AA, Marosi C, Bogdahn U, Curschmann J, Janzer RC, et al. Radiotherapy plus concomitant and adjuvant temozolomide for glioblastoma. N Engl J Med 2005;352:987–96.
4. Wong ET, Hess KR, Gleason MJ, Jaeckle KA, Kyritsis AP, Prados MD, Levin VA, Yung WK. Outcomes and prognostic factors in recurrent glioma patients enrolled onto phase II clinical trials. J Clin Oncol 1999;17:2572–8.

5. Li LH, Fraser TJ, Olin EJ, Bhuyan BK. Action of camptothecin on mammalian cells in culture. Cancer Res 1972;32:2643–50.
6. Gallo RC, Whang-Peng J, Adamson RH. Studies on the antitumor activity, mechanism of action, and cell cycle effects of camptothecin. J Natl Cancer Inst 1971;46:789–95.
7. Friedman HS, Petros WP, Friedman AH, Schaaf LJ, Kerby T, Lawyer J, Parry M, Houghton PJ, Lovell S, Rasheed K, Cloughsey T, Stewart ES, et al. Irinotecan therapy in adults with recurrent or progressive malignant glioma. J Clin Oncol 1999;17:1516–25.
8. Cloughesy TF, Filka E, Kuhn J, Nelson G, Kabbinavar F, Friedman H, Miller LL, Elfring GL. Two studies evaluating irinotecan treatment for recurrent malignant glioma using an every-3-week regimen. Cancer 2003;97:2381–6.
9. Chamberlain MC. Salvage chemotherapy with CPT-11 for recurrent glioblastoma multiforme. J Neurooncol 2002;56:183–8.
10. Prados MD, Lamborn K, Yung WK, Jaeckle K, Robins HI, Mehta M, Fine HA, Wen PY, Cloughesy T, Chang S, Nicholas MK, Schiff D, et al. A phase 2 trial of irinotecan (CPT-11) in patients with recurrent malignant glioma: a North American brain tumor consortium study. Neuro Oncol 2006;8:189–93.
11. Vredenburgh JJ, Desjardins A, Herndon JE, II, Dowell JM, Reardon DA, Quinn JA, Rich JN, Sathornsumetee S, Gururangan S, Wagner M, Bigner DD, Friedman AH, et al. Phase II trial of bevacizumab and irinotecan in recurrent malignant glioma. Clin Cancer Res 2007;13: 1253–9.
12. Vredenburgh JJ, Desjardins A, Herndon JE, II, Marcello J, Reardon DA, Quinn JA, Rich JN, Sathornsumetee S, Gururangan S, Sampson J, Wagner M, Bailey L, et al. Bevacizumab plus irinotecan in recurrent glioblastoma multiforme. J Clin Oncol 2007;25:4722–9.
13. Gradishar WJ. Albumin-bound nanoparticle paclitaxel. Clin Adv Hematol Oncol 2005;3:348–9.
14. Muggia FM. Liposomal encapsulated anthracyclines: new therapeutic horizons. Curr Oncol Rep 2001;3:156–62.
15. Slatter JG, Schaaf LJ, Sams JP, Feenstra KL, Johnson MG, Bombardt PA, Cathcart KS, Verburg MT, Pearson LK, Compton LD, Miller LL, Baker DS, et al. Pharmacokinetics, metabolism, and excretion of irinotecan (CPT-11) following I.V. infusion of [(14)C]CPT-11 in cancer patients. Drug Metab Dispos 2000;28:423–33.
16. Rothenberg ML, Kuhn JG, Burris HA, III, Nelson J, Eckardt JR, Tristan-Morales M, Hilsenbeck SG, Weiss GR, Smith LS, Rodriguez GI, et al. Phase I and pharmacokinetic trial of weekly CPT-11. J Clin Oncol 1993;11:2194–204.
17. Koizumi F, Kitagawa M, Negishi T, Onda T, Matsumoto S, Hamaguchi T, Matsumura Y. Novel SN-38-incorporating polymeric micelles, NK012, eradicate vascular endothelial growth factor-secreting bulky tumors. Cancer Res 2006;66:10048–56.
18. Sumitomo M, Koizumi F, Asano T, Horiguchi A, Ito K, Kakizoe T, Hayakawa M, Matsumura Y. Novel SN-38-incorporated polymeric micelle, NK012, strongly suppresses renal cancer progression. Cancer Res 2008;68:1631–5.
19. Nakajima TE, Yasunaga M, Kano Y, Koizumi F, Kato K, Hamaguchi T, Yamada Y, Shirao K, Shimada Y, Matsumura Y. Synergistic antitumor activity of the novel SN-38-incorporating polymeric micelles, NK012, combined with 5-fluorouracil in a mouse model of colorectal cancer, as compared with that of irinotecan plus 5-fluorouracil. Int J Cancer 2008;122:2148–53.
20. Saito Y, Yasunaga M, Kuroda J, Koga Y, Matsumura Y. Enhanced distribution of NK012, a polymeric micelle-encapsulated SN-38, and sustained release of SN-38 within tumors can beat a hypovascular tumor. Cancer Sci 2008;99:1258–64.
21. Kawato Y, Furuta T, Aonuma M, Yasuoka M, Yokokura T, Matsumoto K. Antitumor activity of a camptothecin derivative, CPT-11, against human tumor xenografts in nude mice. Cancer Chemother Pharmacol 1991;28:192–8.
22. Matsumura Y, Maeda H. A new concept for macromolecular therapeutics in cancer chemotherapy: mechanism of tumoritropic accumulation of proteins and the antitumor agent smancs. Cancer Res 1986; 46:6387–92.
23. Maeda H, Matsumura Y, Kato H. Purification and identification of [hydroxyprolyl3]bradykinin in ascitic fluid from a patient with gastric cancer. J Biol Chem 1988;263:16051–4.
24. Matsumura Y, Maruo K, Kimura M, Yamamoto T, Konno T, Maeda H. Kinin-generating cascade in advanced cancer patients and in vitro study. Jpn J Cancer Res 1991;82:732–41.
25. Dvorak HF, Nagy JA, Dvorak JT, Dvorak AM. Identification and characterization of the blood vessels of solid tumors that are leaky to circulating macromolecules. Am J Pathol 1988;133:95–109.
26. Leung DW, Cachianes G, Kuang WJ, Goeddel DV, Ferrara N. Vascular endothelial growth factor is a secreted angiogenic mitogen. Science 1989;246:1306–9.
27. Abe K, Shoji M, Chen J, Bierhaus A, Danave I, Micko C, Casper K, Dillehay DL, Nawroth PP, Rickles FR. Regulation of vascular endothelial growth factor production and angiogenesis by the cytoplasmic tail of tissue factor. Proc Natl Acad Sci USA 1999;96:8663–8.
28. Belting M, Dorrell MI, Sandgren S, Aguilar E, Ahamed J, Dorfleutner A, Carmeliet P, Mueller BM, Friedlander M, Ruf W. Regulation of angiogenesis by tissue factor cytoplasmic domain signaling. Nat Med 2004;10:502–9.
29. Rong Y, Post DE, Pieper RO, Durden DL, Van Meir EG, Brat DJ. PTEN and hypoxia regulate tissue factor expression and plasma coagulation by glioblastoma. Cancer Res 2005;65:1406–13.
30. Hamada K, Kuratsu J, Saitoh Y, Takeshima H, Nishi T, Ushio Y. Expression of tissue factor correlates with grade of malignancy in human glioma. Cancer 1996;77:1877–83.
31. Takano S, Yoshii Y, Kondo S, Suzuki H, Maruno T, Shirai S, Nose T. Concentration of vascular endothelial growth factor in the serum and tumor tissue of brain tumor patients. Cancer Res 1996;56:2185–90.
32. Chowdhary S, Wong ET. Bevacizumab combined with irinotecan for recurrent glioblastoma multiforme–improvement over available therapy? Nat Clin Pract Neurol 2008;4:242–3.
33. Chamberlain MC Bevacizumab plus irinotecan in recurrent glioblastoma. J Clin Oncol 2008;26:1012–3.
34. Plate KH, Breier G, Weich HA, Risau W. Vascular endothelial growth factor is a potential tumour angiogenesis factor in human gliomas in vivo. Nature 1992;359:845–8.
35. Horten BC, Basler GA, Shapiro WR. Xenograft of human malignant glial tumors into brains of nude mice. A histopatholgical study. J Neuropathol Exp Neurol 1981;40:493–511.
36. Giannini C, Sarkaria JN, Saito A, Uhm JH, Galanis E, Carlson BL, Schroeder MA, James CD. Patient tumor EGFR and PDGFRA gene amplifications retained in an invasive intracranial xenograft model of glioblastoma multiforme. Neuro Oncol 2005;7:164–76.
37. Engebraaten O, Hjortland GO, Hirschberg H, Fodstad O. Growth of precultured human glioma specimens in nude rat brain. J Neurosurg 1999;90:125–32.
38. Galli R, Binda E, Orfanelli U, Cipelletti B, Gritti A, De Vitis S, Fiocco R, Foroni C, Dimeco F, Vescovi A. Isolation and characterization of tumorigenic, stem-like neural precursors from human glioblastoma. Cancer Res 2004;64:7011–21.
39. Gunther HS, Schmidt NO, Phillips HS, Kemming D, Kharbanda S, Soriano R, Modrusan Z, Meissner H, Westphal M, Lamszus K. Glioblastoma-derived stem cell-enriched cultures form distinct subgroups according to molecular and phenotypic criteria. Oncogene 2008;27:2897–909.
40. Onda T, Nakamura I, Seno C, Matsumoto S, Kitagawa M, Okamoto K, Nishikawa K, Suzuki M. Superior antitumor activity of NK012, 7-etyhl-10-hydroxycamptothecin-incorporating micellar nanoparticle, to irinotecan [abstruct 3062]. Proc Am Assoc Cancer Res 2006;47:720s.
41. Kato K, Hamaguchi T, Shirao K, Shimada Y, Doi T, Ohtsu A, Matsumura Y, Yamada Y. Interim analysis of phase I study of NK012, polymer micelle SN-38, in patients with advanced cancer. Proc Am Soc Clin Oncol GI 2008 (Abstract no 485).
42. Burris HA, III, Infante JR, Spigel DR, Greco FA, Thompson DS, Matsumoto S, Kawamura S, Jones SF. A phase I dose-escalation study of NK012. Proc Am Soc Clin Oncol 2008 (Abstract no 2538).

Available online at www.sciencedirect.com
ScienceDirect
Advanced Drug Delivery Reviews 60 (2008) 899–914
Advanced DRUG DELIVERY Reviews
www.elsevier.com/locate/addr

Poly (amino acid) micelle nanocarriers in preclinical and clinical studies ☆

Yasuhiro Matsumura *

Investigative Treatment Division, Research Center for Innovative Oncology, National Cancer Center Hospital East, 6-5-1 Kashiwanoha, Kashiwa City, 277-8577 Japan

Received 18 May 2007; accepted 15 November 2007
Available online 9 February 2008

Abstract

Polymeric micelles are expected to increase the accumulation of drugs in tumor tissues utilizing the EPR effect and to incorporate various kinds of drugs into the inner core by chemical conjugation or physical entrapment with relatively high stability. The size of the micelles can be controlled within the diameter range of 20 to 100 nm, to ensure that the micelles do not pass through normal vessel walls; therefore, a reduced incidence of the side effects of the drugs may be expected due to the decreased volume of distribution.

These are several anticancer agent-incorporated micelle carrier systems under clinical evaluation. Phase 1 studies of a CDDP incorporated micelle, Nc-6004, and an sN-38 incorporated micelle, NK012, are now underway. A phase 2 study of a PTX incorporated micelle, NK105, against stomach cancer is also underway.

Keywords: Poly (amino acid) micelle nanocarrier; Drug delivery system; EPR effect; Clinical trial

Contents

☆ This review is part of the *Advanced Drug Delivery Reviews* theme issue on "Clinical Developments in Drug Delivery Nanotechnology".

* Tel./fax: 81 4 7134 6857.

0169-409X/$ - see front matter © 2008 Elsevier B.V. All rights reserved.
doi:10.1016/j.addr.2007.11.010

1. Preface

Drug delivery system (DDS) could be used for active or passive targeting of tumor tissues. The former refers to the development of monoclonal antibodies directed against tumor-related molecules that allow targeting of the tumor, because of specific binding between the antibody and its antigen. However, the application of DDS using monoclonal antibodies is restricted to tumors expressing high levels of related antigens.

Passive targeting is based on the enhanced permeability and retention (EPR) effect [1]. The EPR effect is based on the pathophysiological characteristics of solid tumor tissues: hypervascularity, incomplete vascular architecture, secretion of vascular permeability factors stimulating extravasation within cancer tissue, and absence of effective lymphatic drainage from tumors that impedes the efficient clearance of macromolecules accumulated in solid tumor tissues.

Several techniques to maximally use the EPR effect have been developed, e.g., modification of drug structures and development of drug carriers. Polymeric micelle-based anticancer drugs were originally developed by Prof. Kataoka et al. in late the 1980s or early 1990s [2–4]. Polymeric micelles were expected to increase the accumulation of drugs in tumor tissues utilizing the EPR effect and to incorporate various kinds of drugs into the inner core by chemical conjugation or physical entrapment with relatively high stability. The size of the micelles can be controlled within the diameter range of 20 to 100 nm, to ensure that the micelles do not pass through normal vessel walls; therefore, a reduced incidence of the side effects of the drugs may be expected due to the decreased volume of distribution.

In this chapter, polymeric micelle systems for which clinical trials are now underway are reviewed.

2. NK105, paclitaxel-incorporating micellar nanoparticle

Paclitaxel(PTX) is one of the most useful anticancer agents known for various cancers, including ovarian, breast, and lung cancers [5,6]. However, PTX has serious adverse effects, e.g., neutropenia and peripheral sensory neuropathy. In addition, anaphylaxis and other severe hypersensitive reactions have been reported to develop in 2–4% of patients receiving the drug even after premedication with antiallergic agents; these adverse reactions have been attributed to the mixture of Cremophor EL and ethanol which was used to solubilize PTX [7,8]. Of the adverse reactions, neutropenia can be prevented or managed effectively by administering a granulocyte colony-stimulating factor. On the other hand, there are no effective therapies to prevent or reduce nerve damage which is associated with peripheral neuropathy caused by PTX; therefore, neurotoxicity constitutes a significant dose-limiting toxicity of the drug [9,10].

2.1. Preparation and characterization of NK105

To construct NK105 micellar nanoparticles (Fig. 1), block copolymers consisting of polyethylene glycol and polyaspartate, so-called PEG-polyaspartate described previously [2–4,11], were used. PTX was incorporated into polymeric micelles formed by physical entrapment utilizing hydrophobic interactions between PTX and the block copolymer polyaspartate chain. After screening of many candidate substances, 4-phenyl-1-butanol was employed for the chemical modification of the polyaspartate block to increase its hydrophobicity. Treating with a condensing agent, 1,3-diisopropylcarbodiimide, the half of carboxyl groups on the polyaspartate were esterified with 4-phenyl-1-butanol. Molecular weight of the polymers was determined to be approximately 20,000, (PEG block: 12,000; modified polyaspartate block: 8000). NK105 was prepared by facilitating the self-association of NK105 polymers and PTX. NK105 was obtained as a freeze-dried formulation and contained ca. 23% (w/w) of PTX, as determined by reversed-phase liquid-chromatography using an ODS column with mobile

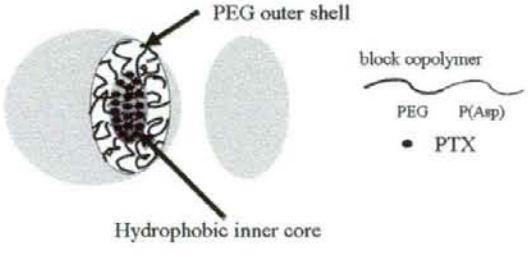

Fig. 1. Preparation and characterization of NK105. The micellar structure of NK105 PTX was incorporated into the inner core of the micelle [29].

Table 1
Pharmacokinetic parameters for the plasma and tumor concentrations of paclitaxel after single intravenous administration of NK105 and PTX to colon 26-bearing CDF1 mice

	Treatment	Dose (mg/kg)	$C_{5\ min}$ (μg/mL)	$t_{1/2}z$ (h)	AUC_{0-t} (μg·h/mL)	AUC_{0-inf} (μg·h/mL)	CL_{tot} (mL/h/kg)	V_{ss} (mL/kg)
Plasma	PTX	50	59.32	0.98	90.2[a)]	91.3	547.6	684.6
	PTX	100	157.67	1.84	309.0[b)]	309.0	323.6	812.2
	NK105	50	1157.03	5.99	7860.9[c)]	7862.3	6.4	46.4
	NK105	100	1812.37	6.82	15565.7[c)]	15573.6	6.4	54.8
			C_{max} (μg/mL)	T_{max} (h)	$t_{1/2}z$ (h)	AUC_{0-t} (μg·h/mL)		AUC_{0-inf} (μg·h/mL)
Tumor	PTX	50	12.50	2.0	7.02	120.8[b)]		133.0
	PTX	100	28.57	0.5	8.06	330.4[c)]		331.0
	NK105	50	42.45	24.0	35.07	2360.1[c)]		3192.0
	NK105	100	71.09	6.0	73.66	3884.9[c)]		7964.5

a) $AUC_{0-6\ h}$; b) $AUC_{0-24\ h}$; c) $AUC_{0-72\ h}$.
Parameters were calculated from the mean value of three or two mice by noncompartmental analysis [12].

phase consisting of acetonitrile and water (9:11, v/v) and detection of ultraviolet absorbance at 227 nm. Finally, NK105, a PTX-incorporating polymeric micellar nanoparticle formulation with a single and narrow size distribution, was obtained. The weight-average diameter of the nanoparticles was approximately 85 nm ranging from 20 to 430 nm [12].

2.2. Pharmacokinetics and pharmacodynamics of NK105

Colon 26-bearing CDF1 mice were given a single i.v. injection of PTX 50 or 100 mg/kg, or of NK105 at an equivalent dose of PTX. Subsequently, the time-course changes in the plasma and tumor levels of PTX were determined in the PTX and NK105 administration groups ; furthermore, the pharmacokinetic parameters of each group were also determined (Table 1). NK105 exhibited slower clearance from the plasma than PTX, while NK105 was present in the plasma for up to 72 h after injection; PTX was not detected after 24 h or later of injection. The plasma concentration at 5 min ($C_{5\ min}$) and the AUC of NK105 were 11- to 20-fold and 50- to 86-fold higher for NK105 than for PTX, respectively. Furthermore, the half-life at the terminal phase ($t_{1/2}z$) was 4 to 6 times longer for NK105 than for PTX. The maximum concentration (C_{max}) and AUC of NK105 in Colon 26 tumors were approximately 3 times and 25 times higher for NK105 than for PTX, respectively. NK105 continued to accumulate in the tumors until 72 h after injection. The tumor PTX concentration was higher than 10 μg/g even at 72 h after the intravenous injection of NK105 50 and 100 mg/kg. By contraries, the tumor PTX concentrations at 72 h after the intravenous administration of free PTX 50 and 100 mg/kg were below detection limits and less than 0.1 μg/g, respectively.

2.3. In vivo antitumor activity

BALB/c mice bearing s.c. HT-29 colon cancer tumors showed decreased tumor growth rates after the administration of PTX and NK105. However, NK105 exhibited superior antitumor activity as compared with PTX ($P<0.001$). The antitumor activity of NK105 administered at a PTX-equivalent dose of 25 mg/kg was comparable to that obtained after the administration of free PTX 100 mg/kg. Tumor suppression by NK105 increased in a dose-dependent manner. Tumors disappeared after the first dosing to mice treated with NK105 at a PTX-equivalent dose of 100 mg/kg, and all mice remained tumor-free thereafter (Fig. 2). In addition, less weight loss was induced in mice which were given NK105 100 mg/kg than in those which were given the same dose of free PTX(data not shown).

2.4. Neurotoxicity of PTX and NK105

Treatment with PTX has resulted in cumulative sensory-dominant peripheral neurotoxicity in humans, characterized clinically by numbness and/or paraesthesia of the extremities. Pathologically, axonal swelling, vesicular degeneration, and demyelination were observed. We, therefore, examined the effects of free PTX and NK105 using both electrophysiological and morphological methods.

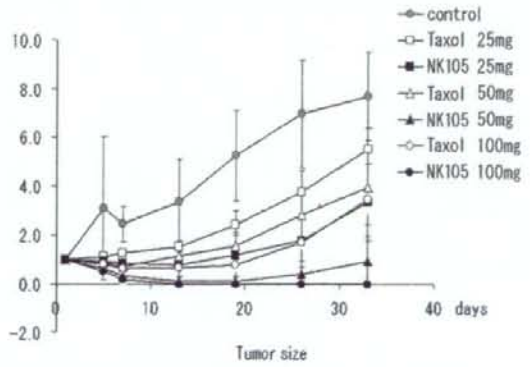

Fig. 2. Effects of PTX (open symbols) and NK105 (closed symbols). PTX and NK105 were injected intravenously once weekly for 3 weeks at PTX-equivalent doses of 25 mg/kg (□, ■), 50 mg/kg (△, ▲), and 100 mg/kg (○, ●), respectively. Saline was injected to animals in the control group (◉) [12].

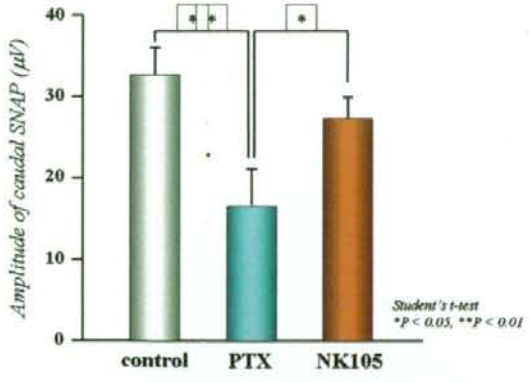

Fig. 3. Effects of PTX or NK105 on the amplitude of rat caudal sensory nerve action potentials as examined 5 days after weekly injections for 6 weeks. Rats (n=14) were injected with NK105 or PTX at a PTX-equivalent dose of 7.5 mg/kg. 5% glucose was also injected in the same manner to animals in the control group [12].

Prior to drug administration, there were no significant differences in the amplitude of caudal sensory nerve action potential (caudal SNAP) between two drug administration groups. On day 6 after the last dosing (at week 6), the amplitude of the caudal SNAP in the control group increased in association with rat maturation. The amplitude was significantly smaller in the PTX group than in the control group ($P<0.01$), while the amplitude was significantly larger in the NK105 group than in the PTX group ($P<0.05$) and was comparable between the NK105 group and the control group (Fig. 3). Histopathological examination of longitudinal paraffin-embedded sections of the sciatic nerve 5 days after the sixth weekly injection revealed degenerative changes. The NK105 administration group showed only a few degenerative myelinated fibers in contrast to the PTX administration group which indicated markedly more numerous degenerative myelinated fibers (data not shown).

2.5. NK105 has more potent radiosensitizing effect than free paclitaxel

Besides the antitumor activity of PTX, its ability to induce radiosensitization has been reported both in vitro [13–16] and *in vivo* [17–19] this effect has been attributed to its effect of stabilizing microtubules and inducing cell cycle arrest at the G2/M phase, the most radiosensitive phase of the cell cycle [20,21]. Since several clinical studies have demonstrated the efficacy of PTX-based chemotherapy combined with radiotherapy, the combined modality is considered to be a potentially important treatment option for lung and breast cancer [22,23].

The adverse effects of radiation, namely, lung toxicities in patients with breast or lung cancer treated by thoracic radiation,

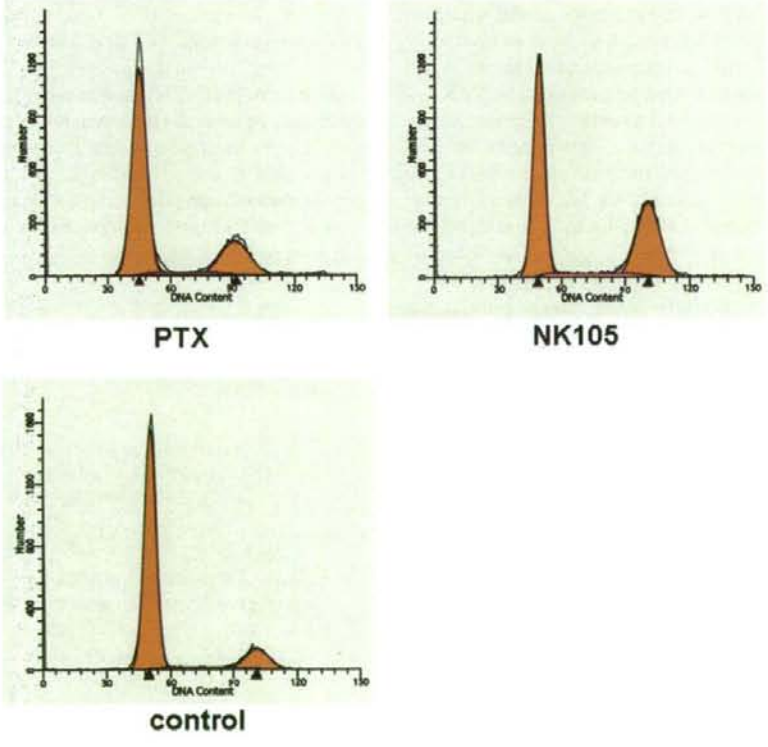

Fig. 4. Cell cycle analysis. Cell cycle analysis of LLC tumor cells 24 h after adding saline as a control, PTX or NK105 [28].

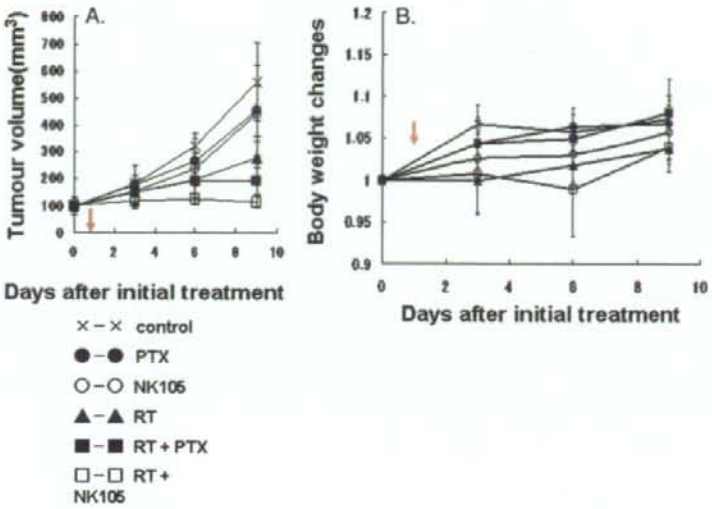

Fig. 5. Antitumor activity. Changes in the LLC tumor growth rates in the mice. (A) Mice receiving TXL-alone(●), NK105-alone(○), combined treatment with PTX and radiation(■), and combined treatment with NK105 and radiation(□) were administered a single i.v. injection of PTX or NK105 at the dose 45 mg/kg. Twenty-four hours after the drugs were administered, the mice in the radiation-alone (Δ)and the combined-treatment groups were irradiated. Mice in the control group (X) were given no treatment. (B) Changes in the relative body weight. Data were derived from the same mice as those used in the present study [28].

are of great concern, and may be dose-limiting or even have a negative impact on the quality of life of the patients, even though radiation is an efficient treatment option. Lung toxicities often result in lung fibrosis, necessitating change of the treatment method and causing much distress or even death of the patients [24,25]. Some clinical trials actually reported an increased incidence of pneumonitis following combined PTX therapy with radiation in patients with breast or lung cancer [26,27].

It is expected that the use of NK105 in place of PTX in combination with radiation may also yield superior results, because of the more potent antitumor activity of this drug as compared to that of free PTX. We evaluated the antitumor activity and severity of lung fibrosis induced by PTX and NK105 administered in combination with thoracic radiation, to examine whether combined NK105 chemotherapy with radiation would be an acceptable or useful treatment modality.

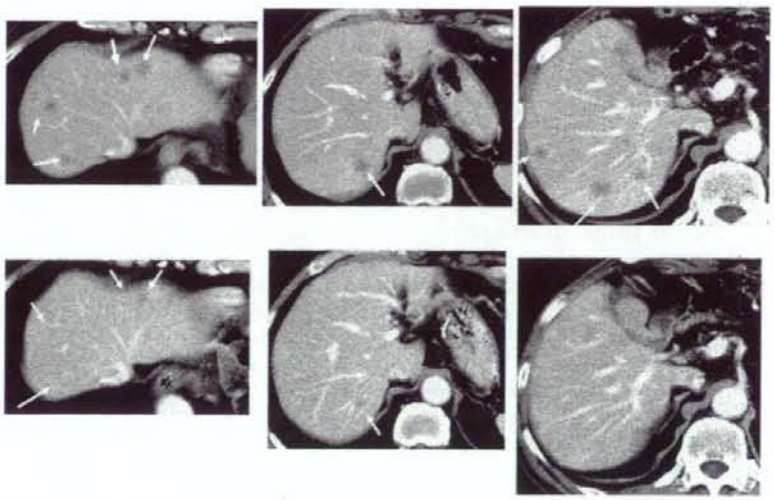

Fig. 6. Serial CT scans. A 60-year-old male with pancreatic cancer who was treated with NK105 at a dose level of 150 mg/m^2. Baseline scan (upper panels) showing multiple metastasis in the liver. Partial response, characterized by a more than 90% decrease in the size of the liver metastasis (lower panels) compared with the baseline scan. The antitumor response was maintained for nearly 1 year [29].

2.5.1. Cell cycle analysis

At 24 h after the administration of PTX or NK105 to the LLC-tumor-bearing mice, severe cell cycle arrest at the G2/M phase was observed in the tumor cells treated with the drugs as compared with that in the control (no drug treatment). There was a tendency towards the NK105-treated LLC tumor cells showing more severe arrest at the G2/M phase than the PTX-treated cells [28] (Fig. 4).

2.5.2. Antitumor activity

Decreased tumor growth rates of the LLC tumors were observed in the mice of the radiation alone, combined PTX with radiation, and combined NK105 with radiation groups [28]. No antitumor activity was observed following treatment with either PTX or NK105 alone, because LLC is primarily a PTX-resistant tumor. Combined NK105 therapy with radiation yielded superior antitumor activity as compared to both radiation alone ($P=0.0047$) and combined PTX therapy with radiation ($P=0.0277$) on the day 9 after the treatment initiation (Fig. 5A). No significant differences in body weight changes were noted among the groups tested (Fig. 5B).

2.5.3. Lung toxicities

Histopathological examination of the lung sections of all the mice receiving radiation showed inflammatory cell infiltration, appearance of intra-alveolar macrophages, and destruction of the alveolar architecture. Major portions of the alveolar septa in the lung sections prepared from the irradiated mice showed slight thickening, although no massive structural destruction was observed. On the other hand, the lung sections prepared from the control non-irradiated group showed no significant histopathological changes. Ashcroft's fibrosis scores in the groups of mice that received radiation ranged from 0.975 to 1.426, with no significant differences among the groups. The score in the control group was nearly zero. In the groups receiving radiation, the severity of lung fibrosis differed significantly among the mice within the same groups, as did the Ashcroft's scores, that is, the S.D. of the Ashcroft's scores in the mice receiving radiation was very high.

2.6. Clinical study

A phase I study was designed to determine maximum tolerated dose (MTD), dose-limiting toxicities (DLTs), the recommended dose (RD) for phase II and the pharmacokinetics of NK105 [29].

NK105 was administered by a 1-hour intravenous infusion every 3 weeks without anti-allergic premedication. The starting dose was 10 mg PTX equivalent/m^2, and dose escalated according to the accelerated titration method.

To date, 17 patients (pts) have been treated at the following doses: 10 mg/m^2 ($n=1$); 20 mg/m^2 ($n=1$); 40 mg/m^2 ($n=1$); 80 mg/m^2 ($n=1$); 110 mg/m^2 ($n=3$); 150 mg/m^2 ($n=5$); 180 mg/m^2 ($n=5$). Tumor types treated have included: pancreatic ($n=9$), bile duct ($n=5$), gastric ($n=2$), and colon ($n=1$). Neutropenia has been the predominant hematological toxicity and grade 3 or 4 neutropenia was observed in pts treated at 110, 150 and 180 mg/m^2. One patient at 180 mg/m^2 developed grade 3 fever. No other

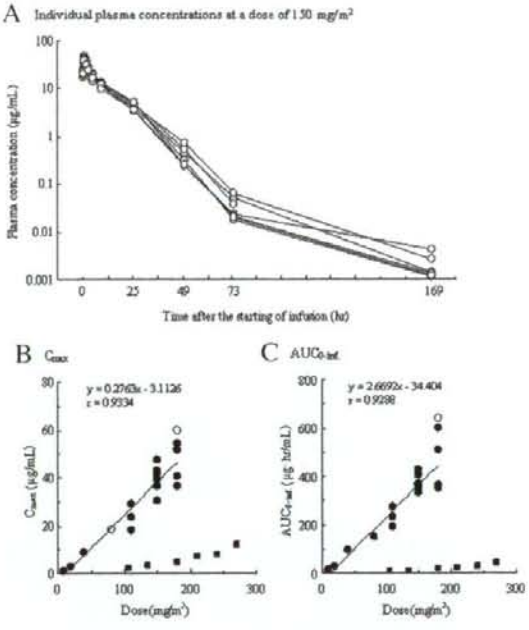

Fig. 7. (A) Individual plasma concentrations of PTX in 7 patients following 1 h intravenous infusion of NK105 at a dose of 150 mg/m^2. Relationships between dose and C_{max} (B), and between dose and AUC_{0-inf} (C) of PTX in patients following 1 h intravenous infusion of NK105. Regression analysis for dose vs. C_{max} was applied using all points except one patient at 80 mg/m^2 whose medication time became 11 min longer and one patient at 180 mg/m^2 who had medication discontinuation and steroid medication. (○) Regression analysis for dose vs. AUC_{0-inf} was applied using all points except one patient who had medication discontinuation and steroid medication. (○) Relationships between dose and C_{max}, and AUC_{0-inf} in patients following conventional PTX administration were plotted (closed square) [29].

grade 3 or 4 non-hematological toxicity including neuropathies was observed. DLTs were observed in pts with at the 180 mg/m^2 (grade 4 neutropenia lasting for more than 5 days), which was determined as MTD. Allergic reactions were not observed in any of the patients except one patient at level. A partial response was observed in one pancreatic cancer pt who received more than 12 courses of NK105 (Fig. 6). Despite of the long time usage, only grade 1 or 2 neuropathy was observed by modifying the dose or period of drug administration. Colon and gastric cancer pts experienced stable disease lasting 10 and 7 courses, respectively. The C_{max} and AUC of NK105 showed dose-dependent characteristics. The plasma AUC of NK105 at 180 mg/m^2 was approximately 30-fold higher than that of commonly-used paclitaxel formulation (Fig. 7).Accrual is ongoing at the 150 mg/m^2 dose level to determine RD. DLT was Grade 4 neutropenia. NK105 generates prolonged systemic exposure to PTX in plasma. Tri-weekly 1-hour infusion of NK105 was feasible and well tolerated, with antitumor activity in pancreatic cancer pt. A phase 2 study of NK105 against stomach cancer is now underway.

3. NC-6004, cisplatin-incorporating micellar nanoparticle

Cisplatin [*cis*-dichlorodiammineplatinum (II): CDDP] is a key drug in the chemotherapy for cancers, including lung,

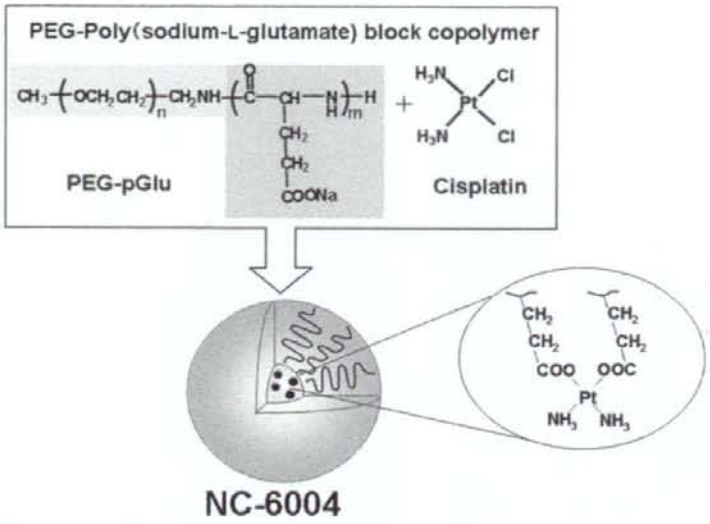

Fig. 8. Preparation and characterization of cisplatin-incorporating polymeric micelles (NC-6004). Chemical structures of cisplatin (CDDP) and polyethylene glycol poly(glutamic acid) block copolymers [PEG-P(Glu) block copolymers], and the micellar structures of CDDP-incorporating polymeric micelles (NC-6004) [39].

gastrointestinal, and genitourinary cancer [30,31]. However, we often find that it is necessary to discontinue treatment with CDDP due to its adverse reactions, e.g., nephrotoxicity and neurotoxicity, despite its persisting effects [32]. Platinum analogues, e.g., carboplatin and oxaliplatin [33], have been developed to date to overcome these CDDP-related disadvantages. Consequently, these analogues are becoming the standard drugs for ovarian cancer [34] and colon cancer [35]. However, those regimens including CDDP are considered to constitute the standard treatment for lung cancer, stomach cancer, testicular cancer [36], and urothelial cancer [37]. Therefore, the development of a drug delivery system (DDS) technology is anticipated, which would offer the better selective accumulation of CDDP into solid tumors while lessening its distribution into normal tissue.

3.1. Preparation and characterization of NC-6004

NC-6004 were prepared according to the slightly modified procedure reported by Nishiyama et al. [38,39] (Fig. 8). NC-6004 consists of polyethylene glycol (PEG), a hydrophilic chain which constitutes the outer shell of the micelles, and the coordinate complex of poly(glutamic acid) (P(Glu)) and CDDP, a polymer–metal complex-forming chain which constitutes the inner core of the micelles. The molecular weight of PEG-P(Glu) as a sodium salt was approximately 18,000 (PEG: 12,000; P (Glu): 6000). The CDDP-incorporated polymeric micelles were clearly discriminated from typical micelles from amphiphilic block copolymers. The driving force of the formation of the CDDP-incorporated micelles is the ligand substitution of platinum(II) atom from chloride to carboxylate in the side chain of P(Glu). The molar ratio of CDDP to the carboxyl groups in the copolymers was 0.71 [38]. A narrowly distributed size of polymeric micelles (30 nm) was confirmed by the dynamic light scattering (DLS) measurement. Also, the static light scattering (SLS) measurement revealed that the CDDP-loaded micelles showed no dissociation upon dilution and the CMC was less than 5×10^{-7}, suggesting remarkable stability compared with typical micelles from amphiphilic block copolymers [38]. It is assumed that the interpolymer cross-linking by Pt(II) atom might contribute to stabilization of the micellar structure.

Table 2
Pharmacokinetic parameter estimates for CDDP and NC-6004 in rats

Compound	Rat	T^a_{max} (h)	C^a_{max} (mg/mL)	$t_{1/2\beta}$ (h)	AUC_{0-t} (mg h/mL)	AUC_{0-inf} (mg h/mL)	CL_{tot} (mL/h/kg)	MRT_{0-inf} (h)	V_{ss} (L/kg)
CDDP	Mean	0.083	11.67	34.50	20.47	75.73	70.67	46.57	3.00
	S.D.		0.57	16.14	2.25	26.13	20.34	22.38	0.61
NC-6004	Mean	0.50	89.90	6.43	1325.90	1335.47	3.77	10.67	0.04
	S.D.		4.29	0.55	77.85	75.99	0.21	0.15	0.0023

See text for definitions of parameters.
The pharmacokinetic parameters were calculated after fitting to a non compartment model using WinNonlin program.
[a]For CDDP group, values of T_{max} and C_{max} represent 5 min and $C_{5\ min}$, respectively [39].

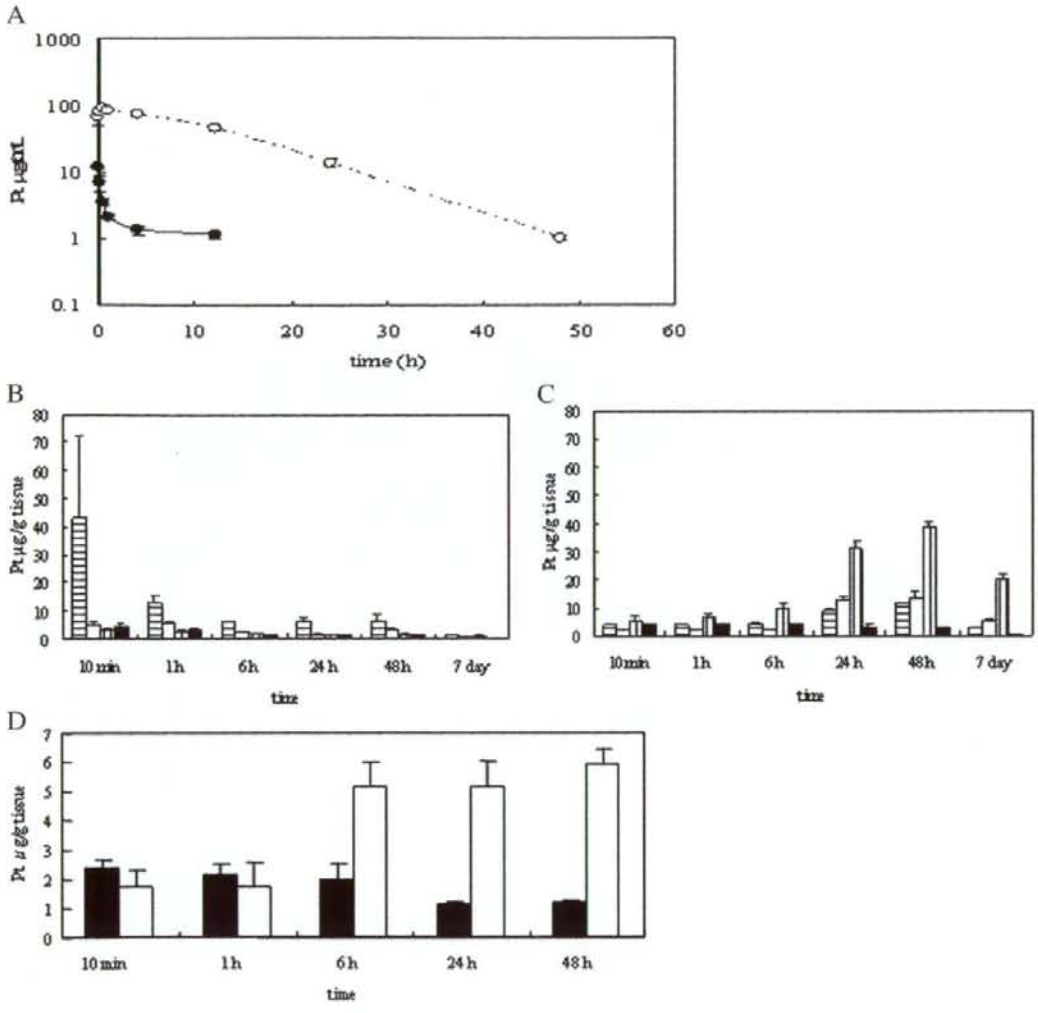

Fig. 9. Time profiles of platinum (Pt) concentration in the plasma and tissue distribution of Pt after a single i.v. injection of CDDP (5 mg/kg) or NC-6004 (an equivalent dose of 5 mg/kg CDDP). (A) Concentration-time profile of Pt in the plasma after a single i.v. injection of CDDP (●) and NC-6004 (○) in rats ($n=3$). Tissue distribution of platinum after a single i.v. injection of CDDP (B) and NC-6004 (C) in rats ($n=3$) (kidney (▥), liver (□), spleen (▤), and lung (■)). (D) Time profiles of platinum concentration in the MKN-45 solid tumor after a single i.v. injection of CDDP (■) and NC-6004 (□) in MKN-45 bearing BALB/c nude mice ($n=3$). Values are expressed as the mean±S.D [39].

The release rates of CDDP from NC-6004 were 19.6% and 47.8% at 24 and 96 h, respectively. In distilled water, furthermore, NC-6004 was stable without releasing cisplatin.

3.2. Pharmacokinetics and pharmacodynamics

FAAS could measure serum concentrations of platinum up to 48 h after i.v. injection of NC-6004 but could measure them only up to 4 h after i.v. injection of CDDP. NC-6004 showed a very long blood retention profile as compared with CDDP [39]. The AUC_{0-t} and C_{max} values were significantly higher in animals given NC-6004 than in animals given CDDP, namely, 65-fold and 8-fold, respectively ($P<0.001$ and $P<0.001$, respectively) (Table 2, Fig. 9A). Furthermore, the CL_{tot} and V_{ss} values were significantly lower in animals given NC-6004 than in animals given CDDP, i.e., one-nineteenth and one-seventy fifth, respectively ($P<0.01$ and $P<0.01$, respectively) (Table 2).

Regarding the concentration-time profile of platinum in various tissues after i.v. injection of CDDP or NC-6004, all organs measured exhibited the highest concentrations of platinum within 1 h after administration in all animals given CDDP (Fig. 9B). Furthermore, animals given NC-6004 exhibited the highest tissue concentrations of platinum in the liver and spleen at late time points (24 and 48 h after administration, respectively). However, the concentrations decreased on day 7 after administration (Fig. 9C). In addition, and in a similar manner to other drugs which are incorporated in polymeric carriers, NC-6004 demonstrated accumulation in organs of the

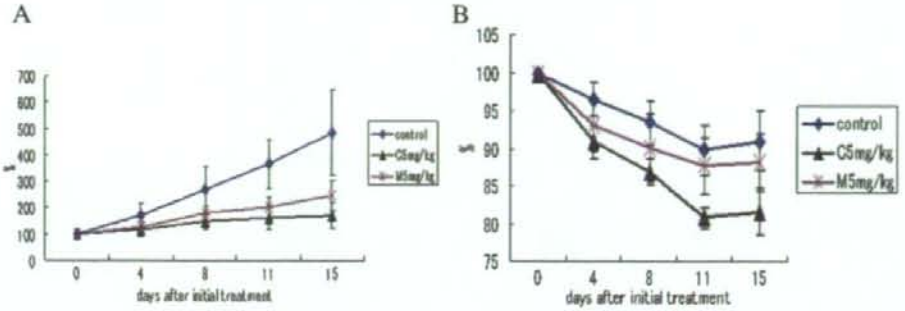

Fig. 10. Relative changes in MKN-45 tumor growth rates in nude mice. (A) CDDP(▲) and NC-6004(X) were injected intravenously every 3 days, 3 administrations in total, at CDDP-equivalent doses of 5 mg/kg. 5% glucose was injected in the control mice (◇). (B) Changes in relative body weight. Data were derived from the same mice as those used in the present study. Values are expressed as the mean±S.E [39].

reticuloendothelial system, e.g., liver and spleen. At 48 h after administration, tissue concentrations of platinum in the liver and spleen were 4.6- and 24.4-fold higher for NC-6004 than for CDDP. On the other hand, a marked increase in tissue platinum concentration was observed immediately after administration in the kidneys of animals given CDDP. Renal platinum concentration at 10 min and 1 h after administration were 11.6- and 3.1-fold lower, respectively, in animals given NC-6004 than in animals given CDDP. Furthermore, the maximum concentration (C_{max}) in the kidney was 3.8-fold lower at the time of NC-6004 administration than at the time of CDDP administration.

Regarding the tumor accumulation of platinum, tumor concentrations of platinum peaked at 10 min after administration of CDDP. On the other hand, tumor concentrations of platinum peaked at 48 h after administration of NC-6004 (Fig. 9D). The maximum concentration (C_{max}) in tumor was 2.5-fold higher for NC-6004 than for CDDP ($P<0.001$). Furthermore, the tumor AUC was 3.6-fold higher for NC-6004 than for CDDP (81.2 μg/mL h and 22.6 μg/mL h in animals given NC-6004 and CDDP, respectively).

3.3. In vivo antitumor activity

BALB/c nude mice implanted with a human gastric cancer cell line MKN-45 showed decreased tumor growth rates after i.v. injection of CDDP and NC-6004 (Fig. 10A). In the administration of CDDP, the CDDP 5 mg/kg administration group showed a significant decrease ($P<0.01$) in tumor growth rate as compared with the control group. However, the NC-6004 administration groups at the same dose levels as CDDP showed no significant difference in tumor growth rate. Regarding time-course changes in body weight change rate, the CDDP 5 mg/kg administration group showed a significant decrease ($P<0.001$) in body weight as compared with the control group. On the other hand, NC-6004 administration group did not show a decrease in body weight as compared with the control group (Fig. 10B).

3.4. Nephrotoxicity of CDDP and NC-6004

In the CDDP 10 mg/kg administration group, 4 of 12 rats died from toxicity within 7 days after drug administration. No deaths occurred in the NC-6004 10 mg/kg administration group. Regarding renal function, the BUN concentrations on day 7 after the administration of 5% glucose, CDDP 10 mg/kg, and NC-6004 10 mg/kg were 20.8±3.0, 65.3±44.4, and 20±4.5 mg/dL, respectively. The plasma concentrations of creatinine on day 7 after the administration of 5% glucose, CDDP 10 mg/kg, and NC-6004 10 mg/kg were 0.27±0.03, 0.68±0.23, and 0.28±0.04 mg/dL, respectively. The CDDP 10 mg/kg administration group showed significantly higher plasma concentrations of BUN and creatinine as compared with the control group ($P<0.05$ and $P<0.001$, respectively), with the NC-6004 10 mg/kg administration group ($P<0.05$ and $P<0.001$, respectively) (Fig. 11A and B). Light microscopy indicated tubular dilation with flattening of the lining cells of the tubular epithelium in the kidney from all animals in the CDDP 10 mg/kg administration group. On the other hand, no histopathological change was observed in the kidneys from all animals in the NC-6004 10 mg/kg administration group.

3.5. Neurotoxicity of CDDP and NC-6004

Neurophysiological examination revealed that motor nerve conduction velocities (MNCVs) in animals given 5% glucose, CDDP, and NC-6004 were 44.2±3.5, 40.94±5.08, and 40.62±0.63 m/s, respectively. No significant difference was found among the groups with respect to MNCV. Furthermore, sensory

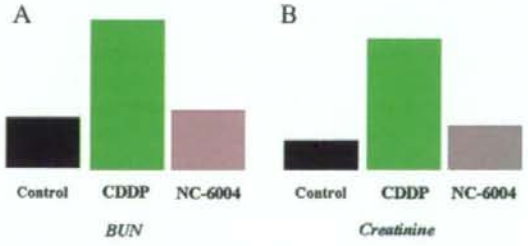

Fig. 11. Nephrotoxicity of CDDP and NC-6004. Plasma concentrations of blood urea nitrogen (BUN) and creatinine were measured after a single i.v. injection of 5% glucose ($n=8$), CDDP at a dose of 10 mg/kg ($n=12$), NC-6004 at a dose of 10 mg/kg ($n=13$) on a CDDP basis (modification of ref. [39]).

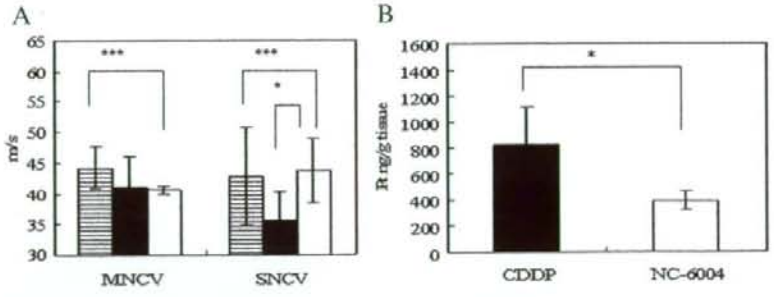

Fig. 12. Neurotoxicity of CDDP and NC-6004 in rats. Rats ($n=5$) were given CDDP (2 mg/kg), NC-6004 (an equivalent dose of 2 mg/kg CDDP), or 5% glucose, all intravenously twice a week, 11 administrations in total. Sensory nerve conduction velocity (SNCV) and motor nerve conduction velocity (MNCV) of the sciatic nerve at week 6 after the initial administration (A). The platinum concentration in the sciatic nerve. Rats were given CDDP (5 mg/kg, $n=5$), NC-6004 (an equivalent dose of 5 mg/kg CDDP, $n=5$), or 5% glucose ($n=2$), all intravenously twice a week, 4 administrations in total. On day 3 after the final administration, a segment of the sciatic nerve was removed and the platinum concentration in the sciatic nerve was measured by ICP-MS (B). The data are expressed as the mean±S.D. *: $P<0.05$ [39].

nerve conduction velocities (SNCVs) in animals given 5% glucose, CDDP, and NC-6004 were 42.86±8.07, 35.48±4.91, and 43.74±5.3 m/s, respectively. Animals given NC-6004 showed no delay in SNCV as compared with animals given 5% glucose. On the other hand, animals given CDDP showed a significant delay ($P<0.05$) in SNCV as compared with animals given NC-6004 (Fig. 12A). The analysis by ICP-MS on sciatic nerve concentrations of platinum could not detect platinum in the sciatic nerve from animals given 5% glucose (data not shown). Sciatic nerve concentrations of platinum in animals given CDDP and NC-6004 were 827.2±291.3 and 395.5± 73.1 ng/g tissue. Therefore, the concentrations were significantly ($P<0.05$) lower in animals given NC-6004 (Fig. 12B). This finding is believed to be a factor which reduced neurotoxicity following NC-6004 administration as compared with the CDDP administration.

3.6. Present situation of a clinical study of NC-6004

A phase 1 clinical trial of NC-6004 is now under way in United Kingdom. Starting dose of NC-6004 was 10 mg/m2. NC-6004 was administered once every 3 weeks with only 1000 ml water loading. In Japan, a phase 1 trial will be stared soon in the National Cancer Center Hospital.

4. NK012, SN-38-incorporating micellar nanoparticle

The antitumor plant alkaloid camptothecin (CPT) is a broad-spectrum anticancer agent which targets the DNA topoisomerase I. Although CPT has showed promising antitumor activity *in vitro* and *in vivo* [40,41], it has not been used clinically because of its low therapeutic efficacy and severe toxicity [42,43]. Among CPT analogs, irinotecan hydrochloride (CPT-11) has recently been demonstrated to be active against colorectal, lung, and ovarian cancer [44–48]. CPT-11 itself is a prodrug and is converted to 7-ethyl-10-hydroxy-CPT (SN-38), a biologically active metabolite of CPT-11, by carboxylesterases (CEs). SN-38 exhibits up to 1000-fold more potent cytotoxic activity against various cancer cells *in vitro* than CPT-11 [49]. Although CPT-11 is converted to SN-38 in the liver and tumor, the metabolic conversion rate is less than 10% of the original volume of CPT-11 [50,51]. In addition, the conversion of CPT-11 to SN-38 depends on the genetic inter-individual variability of CE activity [52]. Thus, direct use of SN-38 might be of great advantage and attractive for cancer treatment. For the clinical use of SN-38, however it is essential to develop a soluble form of water-insoluble SN-38. The progress of the manufacturing technology of "micellar nanoparticles" may make it possible to use SN-38 for *in vivo* experiments and further clinical use.

4.1. Preparation and characterization of NK012

NK012 is an SN-38-loaded polymeric micelle constructed in an aqueous milieu by the self-assembly of an amphiphilic block copolymers, PEG-PGlu(SN-38) [53]. The molecular weight of PEG-PGlu(SN-38) was determined to be approximately 19,000 (PEG segment: 12,000; SN-38-conjugated PGlu segment: 7,000). NK012 was obtained as a freeze-dried formulation and contained ca. 20% (w/w) of SN-38 (Fig. 13A). The mean particle size of NK012 is 20 nm in diameter with a relatively narrow range (Fig. 13B). The releasing rates of SN-38 from NK012 in phosphate buffered saline at 37 °C were 57% and 74% at 24 h and 48 h, respectively, and that in 5% glucose solution at 37 °C were 1% and 3% at 24 h and 48 h, respectively (Fig. 13C). These results indicate that NK012 can release SN-38 under neutral condition even without the presence of a hydrolytic enzyme, and is stable in 5% glucose solution. It is suggested that NK012 is stable before administration and starts to release SN-38, the active component, under physiological conditions after administration.

4.2. Cellular sensitivity of NSCLC and colon cancer cells to SN-38, NK012, and CPT-11

The IC_{50} values of NK012 for the cell lines ranged from 0.009 μM (Lovo cells) to 0.16 μM (WiDR cells). The growth-inhibitory effects of NK012 are 43–340-fold more potent than those of CPT-11, whereas the IC_{50} values of NK012 were 2.3–5.8-fold higher than those of SN-38.NK012 exhibited a higher